*Electronic Supplementary Material (ESI) for Journal of Materials Chemistry A.*

# Bimetallic-ions co-intercalation to stabilize vanadium-oxygen bond towards high-performance aqueous zinc-ion storage

*Yulin Jiang,[a] Xia Wen,[a] Yinuo Li,[a] Yuhang Li,[a] Yanan Peng,[a] Wang Feng,[a] Xiaohui Li,[a] Junbo Yang,[a] Luying Song,[a] Ling Huang,[a] Hang Sun[a] and Jianping Shi*[a]*

[a] The Institute for Advanced Studies, Wuhan University, Wuhan 430072, China.
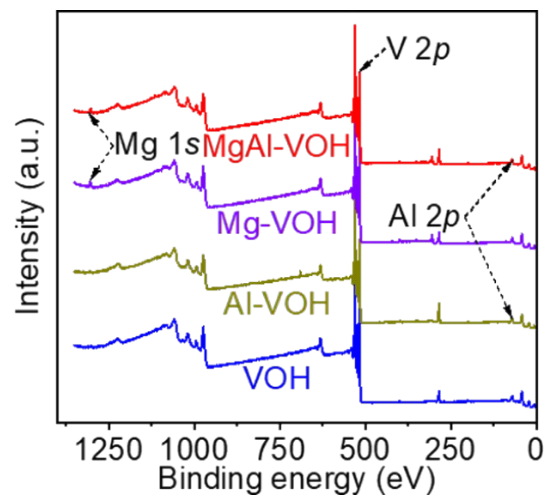*Email: jianpingshi@whu.edu.cn

Fig. S1 XPS spectra of MgAl-VOH, Mg-VOH, Al-VOH, and pure VOH. The coexistence of Mg and Al signals indicates the successful achievement of MgAl-VOH using the unique bimetallic-ions co-intercalated strategy.
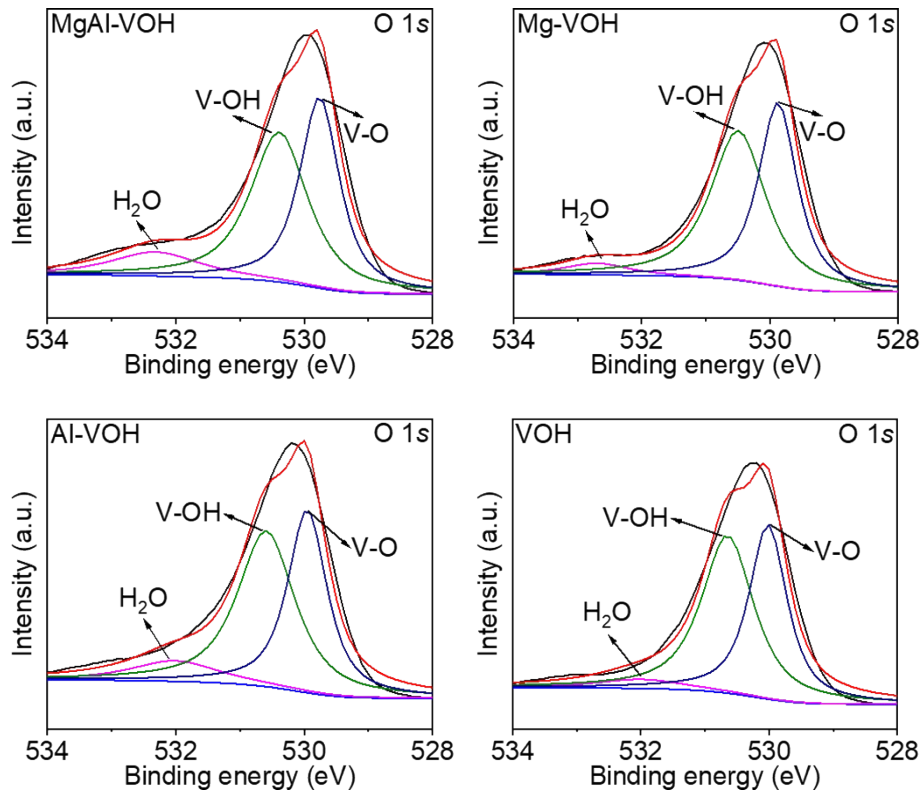
Fig. S2 O 1*s* XPS spectra of MgAl-VOH, Mg-VOH, Al-VOH, and pure VOH. The Al-O and Mg-O peaks are not observed in such samples, implying that $Mg^{2+}$ and $Al^{3+}$ ions are intercalated rather than doped in VOH.
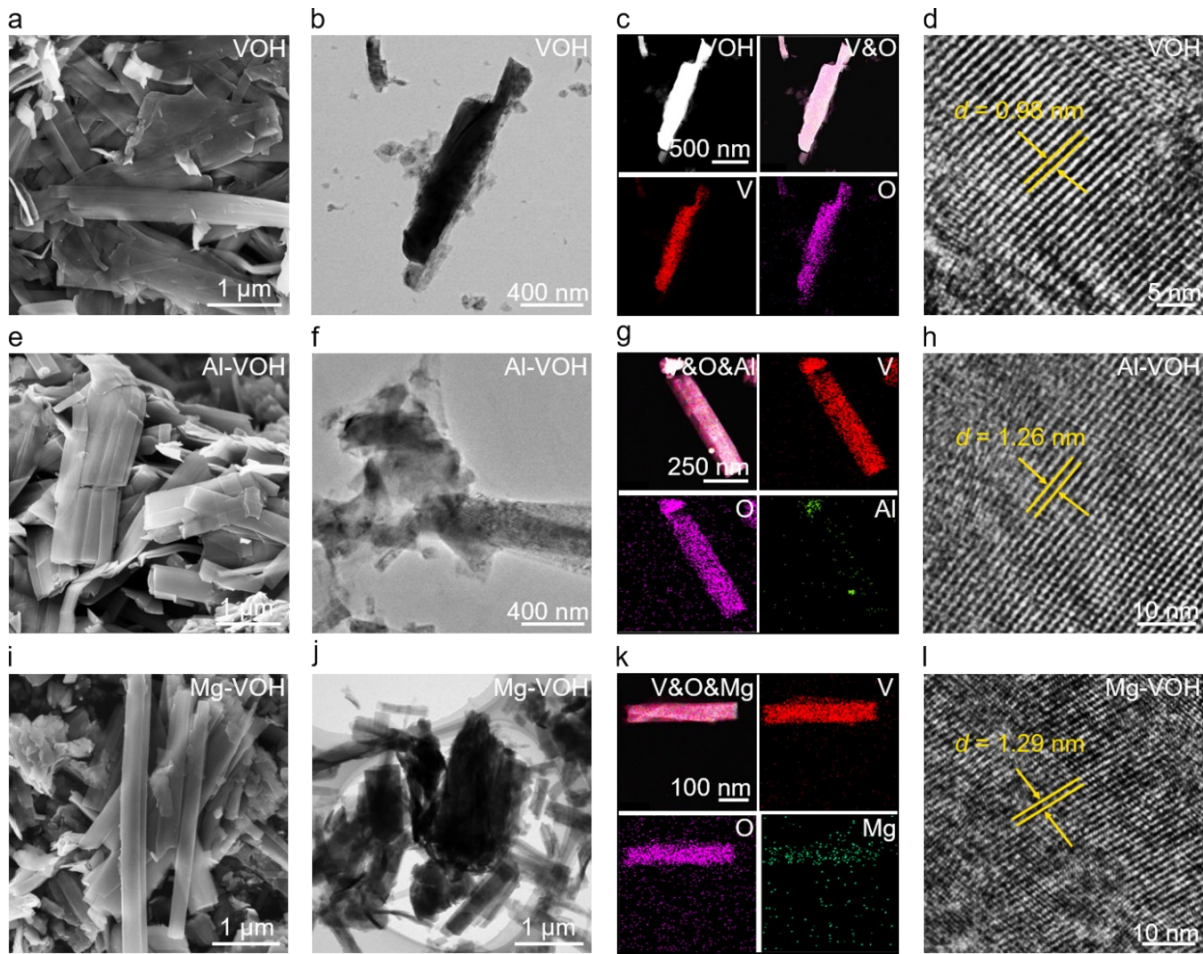
Fig. S3 The morphologies and chemical compositions characterizations of Mg-VOH, Al-VOH, and pure VOH. (a,e,i) SEM images of Mg-VOH, Al-VOH, and pure VOH, showing their nanobelt morphologies. (b,f,j) TEM images of Mg-VOH, Al-VOH, and pure VOH. (c,g,k) EDS mapping images of Mg-VOH, Al-VOH, and pure VOH, revealing their uniform elements distributions. (d,h,l) Atomic resolution TEM images of Mg-VOH, Al-VOH, and pure VOH. The large interlayer spacings are observed in Mg-VOH (1.29 nm) and Al-VOH (1.26 nm) comparing with the pure VOH (0.98 nm).
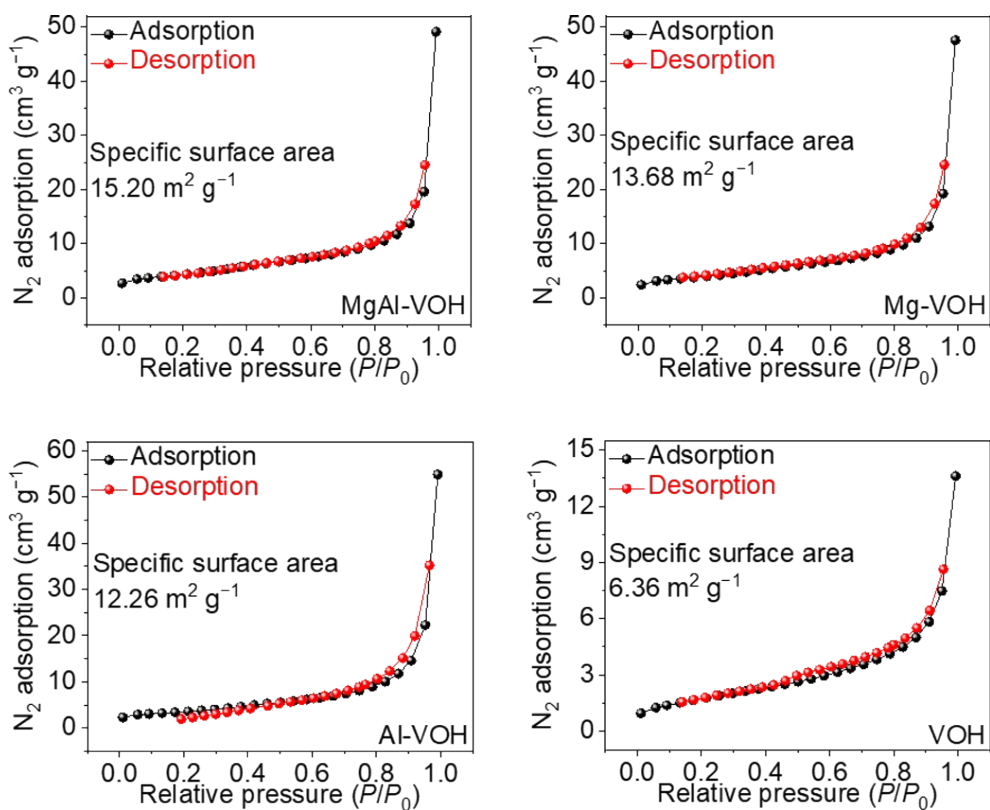
Fig. S4 The specific surface area calculations for MgAl-VOH, Mg-VOH, Al-VOH, and pure VOH.
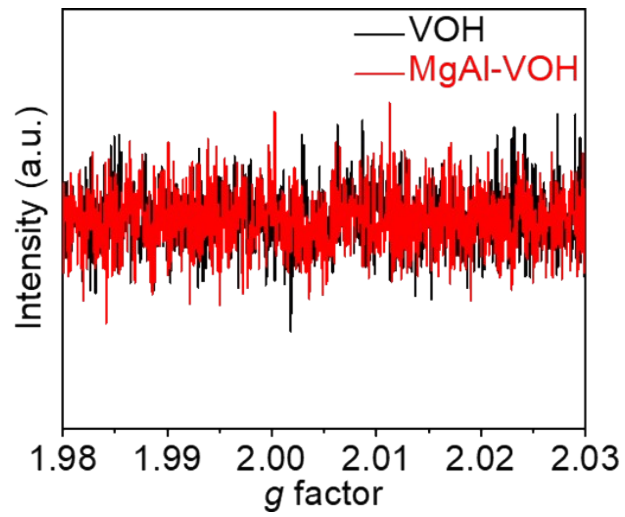
Fig. S5 EPR spectra of MgAl-VOH and pure VOH, showing that the oxygen vacancies are not observed after introducing $Al^{3+}$ and $Mg^{2+}$ ions.
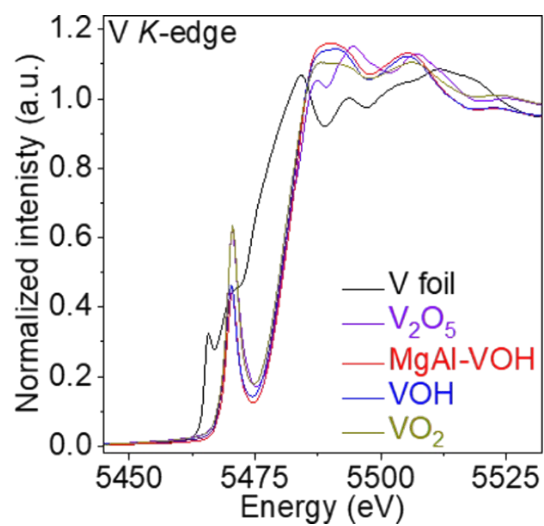
Fig. S6 XANES spectra of MgAl-VOH, VOH, V foil, $V_2O_5$, and $VO_2$, respectively. The existence and low strength of pre-edge in MgAl-VOH indicates the abundant $3d$ electrons of V.
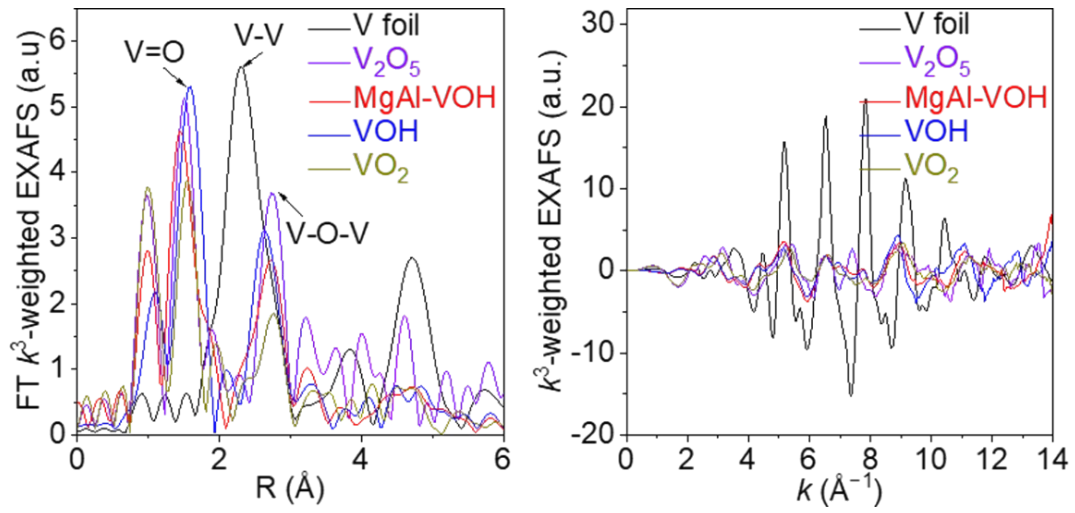
Fig. S7 EXAFS measurement results of MgAl-VOH, VOH, V foil, V$_2$O$_5$, and VO$_2$, respectively. The smaller V=O bond length in MgAl-VOH than that in VOH should stabilize the V=O bonds significantly.

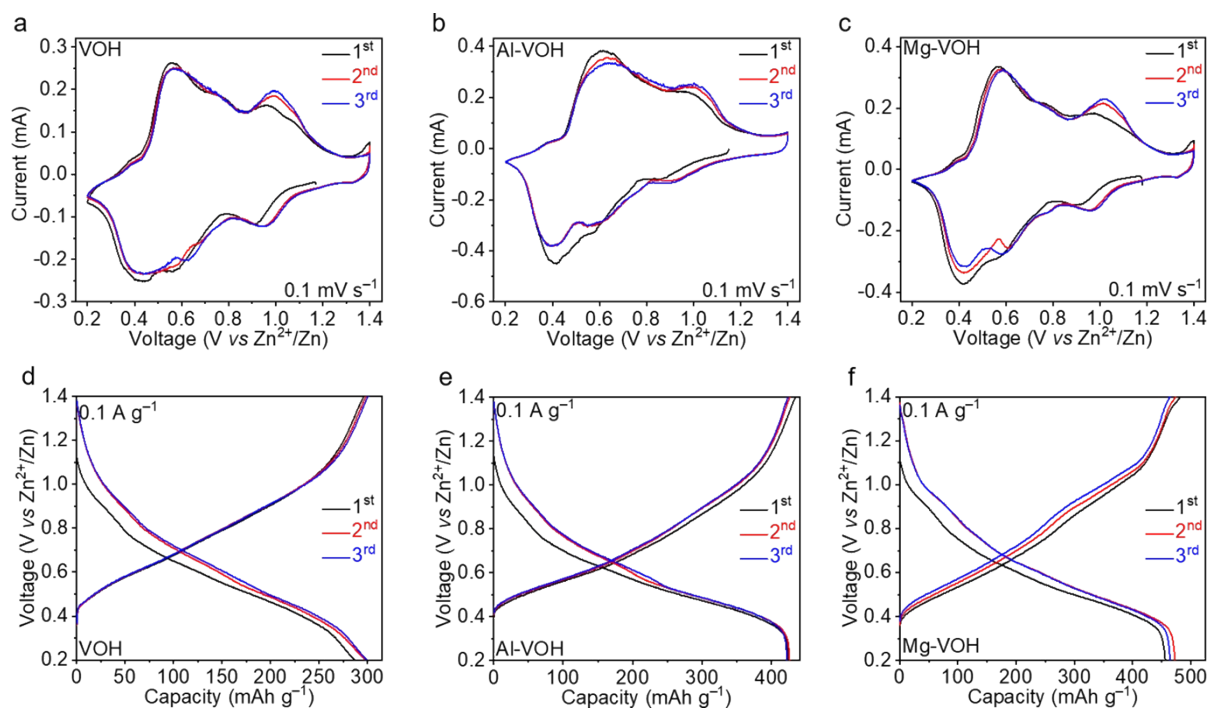Fig. S8 Electrochemical performances of Mg-VOH, Al-VOH, and pure VOH. (a−c) CV curves of Mg-VOH, Al-VOH, and pure VOH in the first three cycles with a scan rate of 0.1 mV s$^{-1}$. (d−f) Charging and discharging curves of Mg-VOH, Al-VOH, and pure VOH in the first three cycles at a current density of 0.1 A g$^{-1}$.
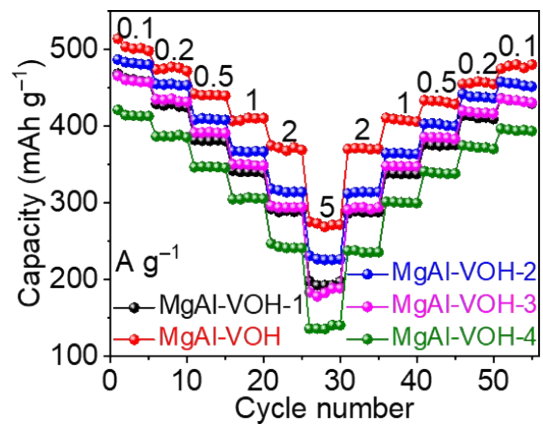
Fig. S9 Rate capabilities of MgAl-VOH with different $Mg^{2+}$ and $Al^{3+}$ ions concentrations.
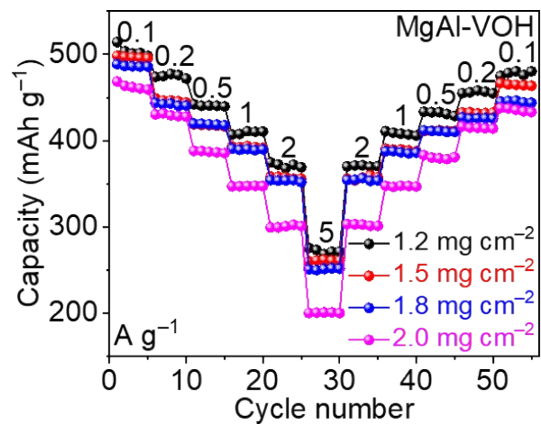
Fig. S10 Rate capabilities of MgAl-VOH with the mass loadings of 1.2, 1.5, 1.8, and 2.0 mg cm$^{-2}$, respectively.
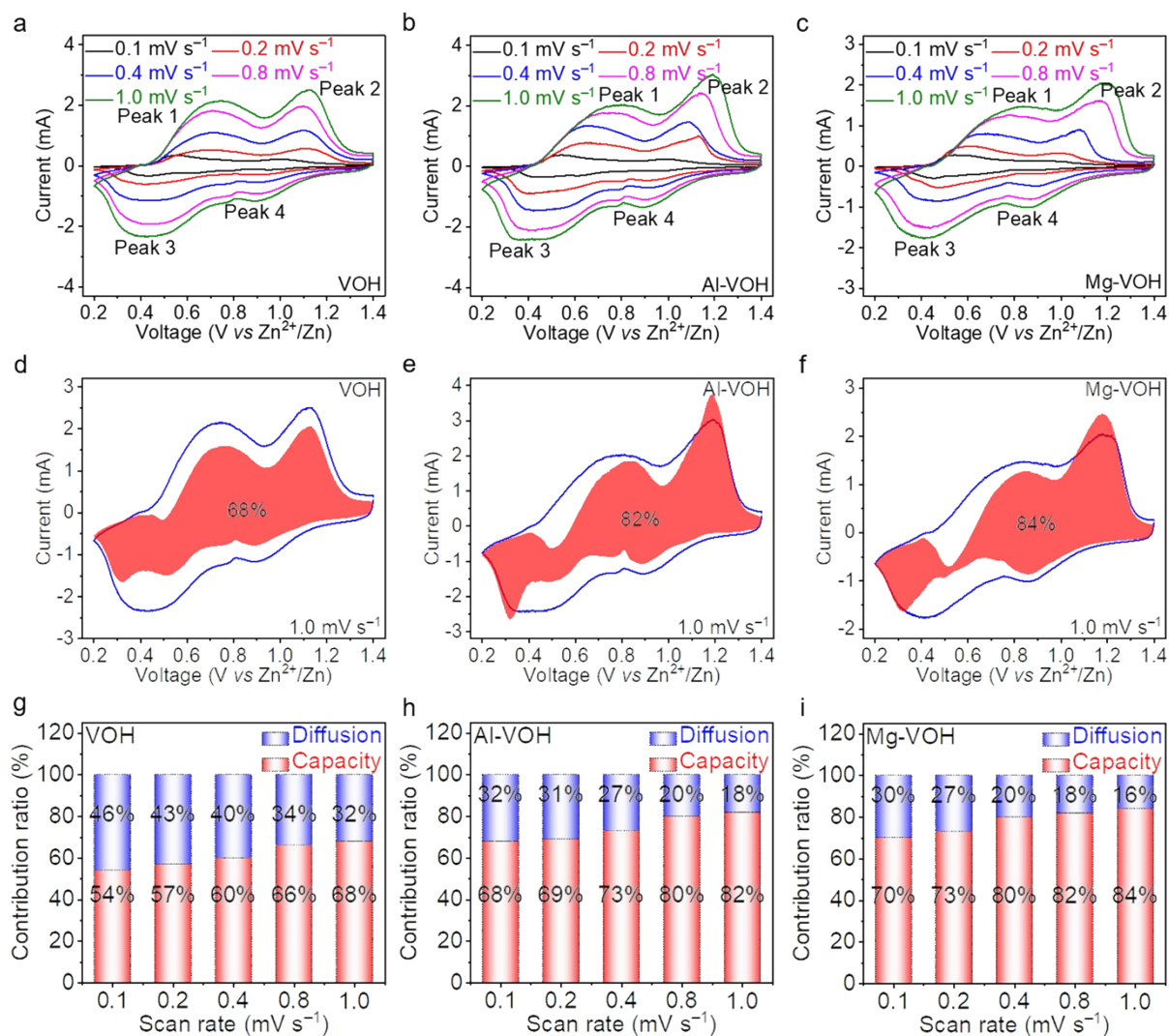
Fig. S11 Electrochemical kinetics of Mg-VOH, Al-VOH, and pure VOH. (a−c) CV curves of Mg-VOH, Al-VOH, and pure VOH at different scan rates. (d−f) CV profiles of Mg-VOH, Al-VOH, and pure VOH with the capacitive contribution at a scan rate of 1.0 mV s$^{-1}$. (g−i) Capacitive contributions in Mg-VOH, Al-VOH, and pure VOH at different scan rates.
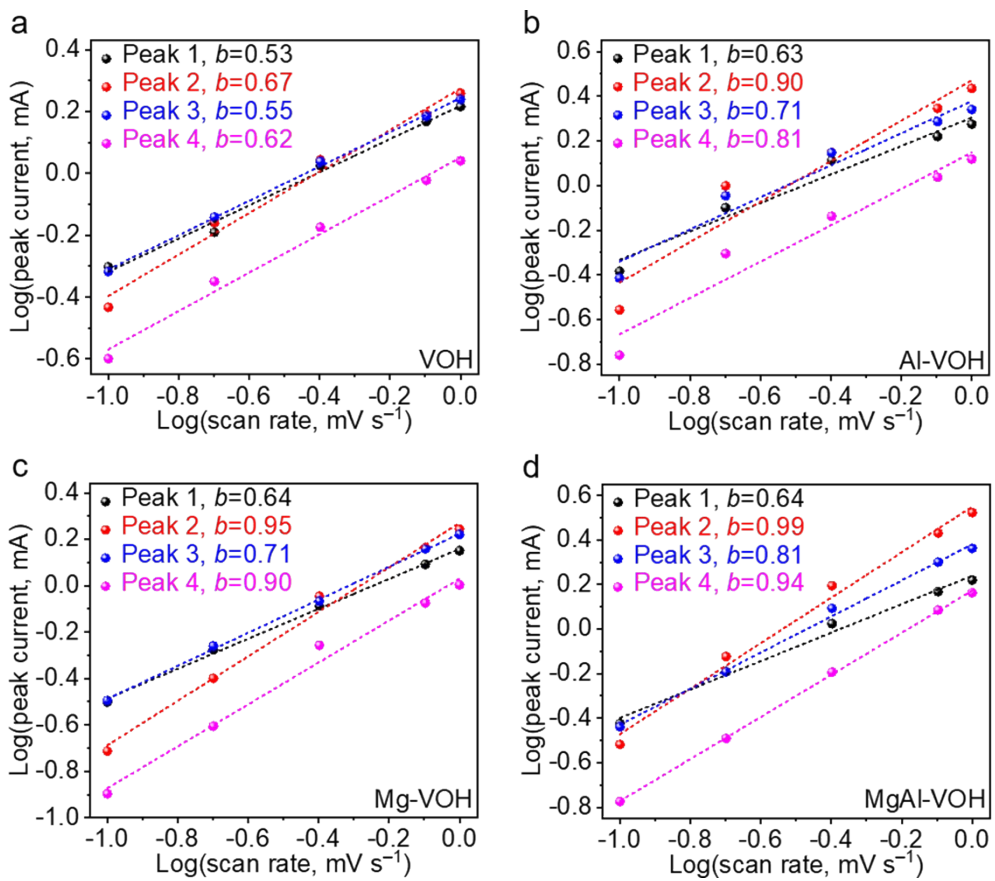
Fig. S12 The extraction of capacitive contribution for MgAl-VOH, Mg-VOH, Al-VOH, and pure VOH, respectively. (a−d) The *b* values of such four electrodes.
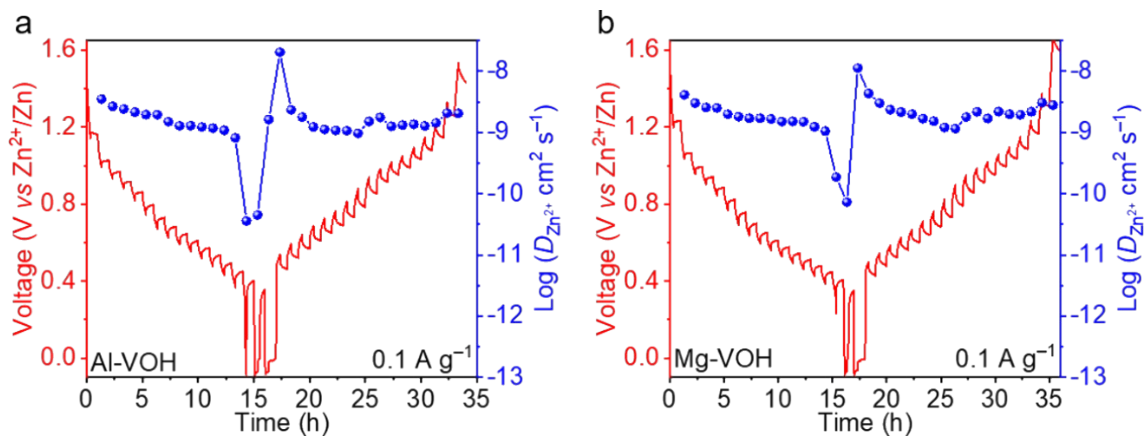
Fig. S13 $Zn^{2+}$ ion diffusion coefficients in Mg-VOH and Al-VOH during the charging and discharging processes.
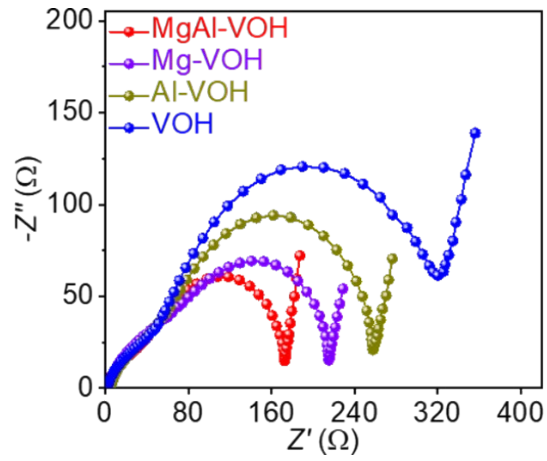
Fig. S14 EIS results of MgAl-VOH, Mg-VOH, Al-VOH, and pure VOH. The smaller resistance in MgAl-VOH than those in Mg-VOH, Al-VOH, and pure VOH indicates the faster charge transfer.
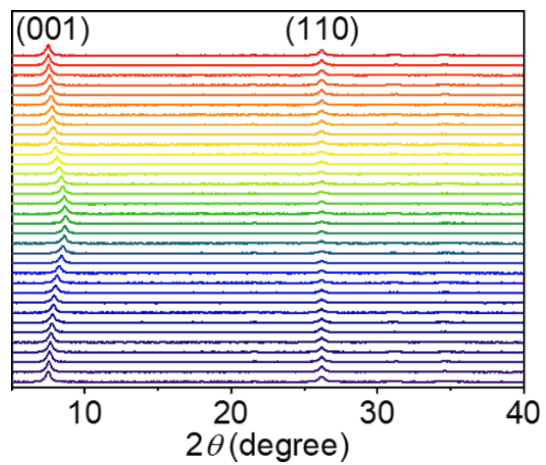
Fig. S15 In-situ XRD patterns of MgAl-VOH during the charging and discharging processes. The unchanged (110) characteristic peak indicates the high structure stability of MgAl-VOH.
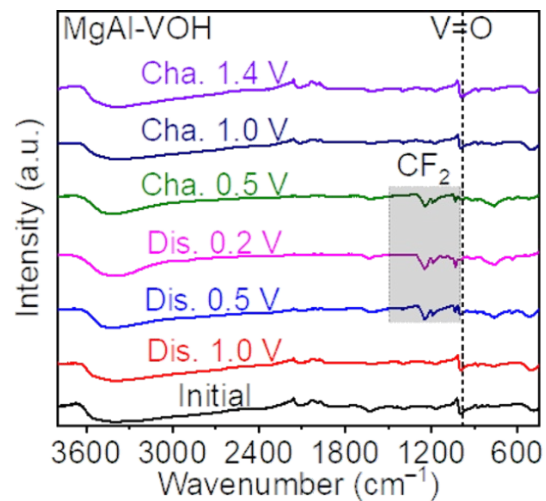
Fig. S16 Ex-situ FTIR of MgAl-VOH at different charging and discharging states. The formation of $Zn_x(OH)_y(CF_3SO_3)_{2x-y} \cdot nH_2O$ by-product confirms the co-de/intercalation mechanism of $Zn^{2+}/H^+$ ions.
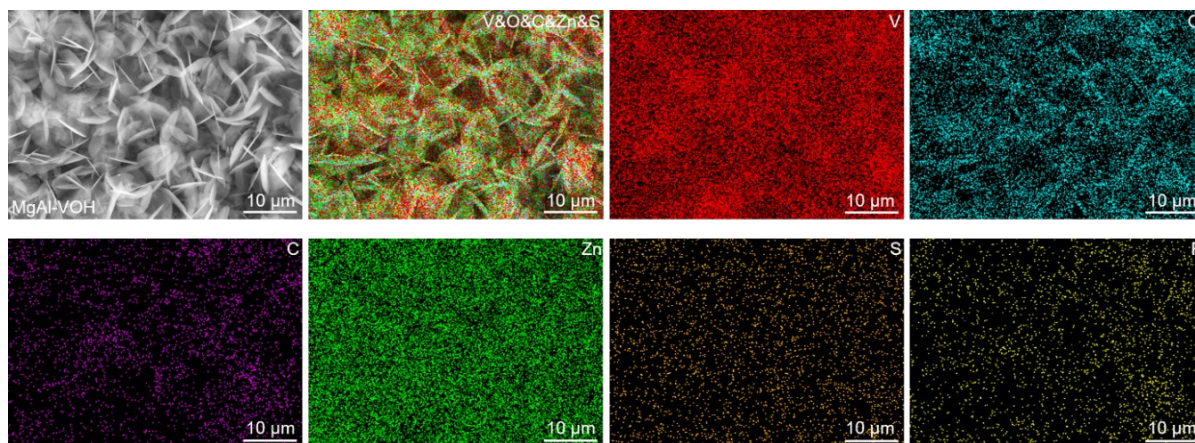
Fig. S17 EDS mapping images of MgAl-VOH after discharging to 0.2 V, reconfirming the co-de/intercalation mechanism of $Zn^{2+}/H^+$ ions.
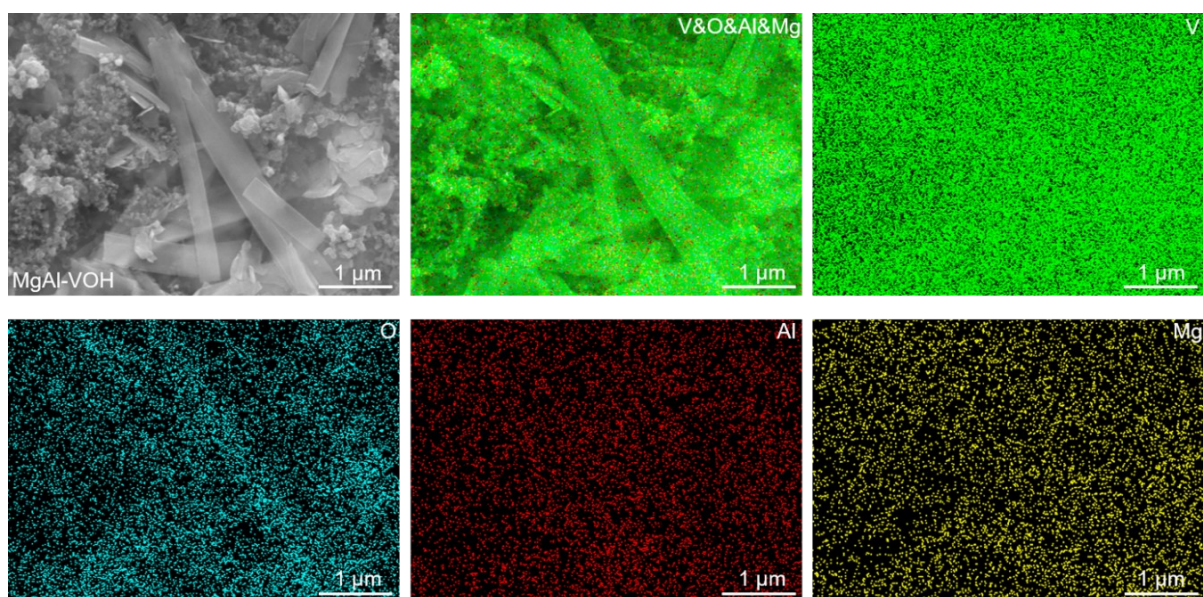
Fig. S18 EDS mapping images of MgAl-VOH at the initial state, showing the uniform distributions of Mg, Al, V, and O elements.
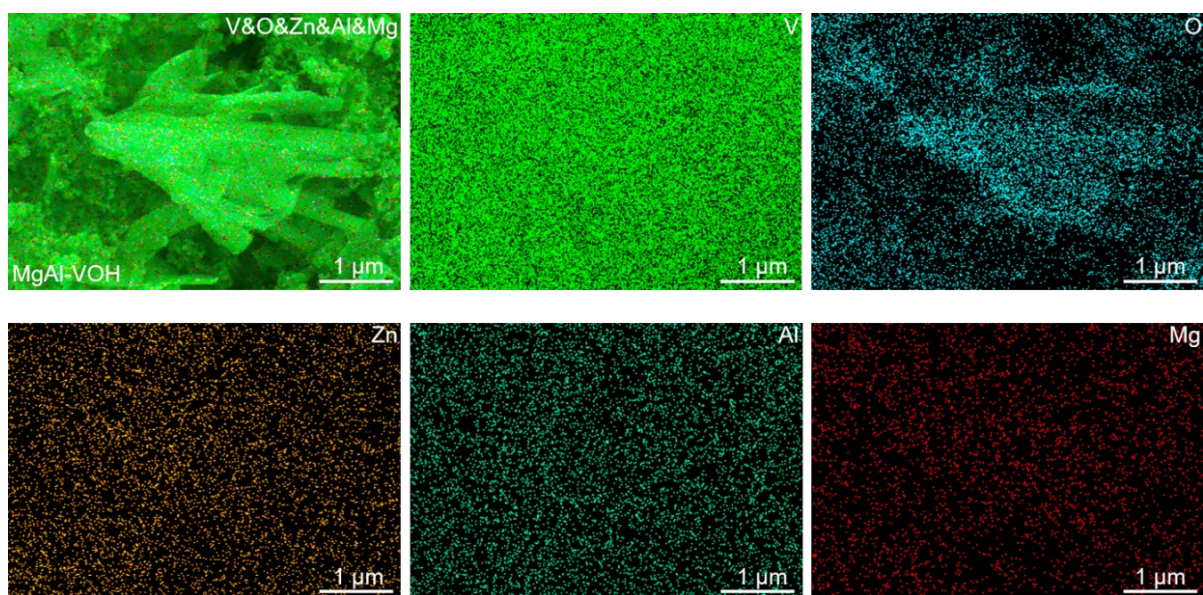
Fig. S19 EDS mapping images of MgAl-VOH after charging to 1.4 V, revealing its robust structure.

VOH
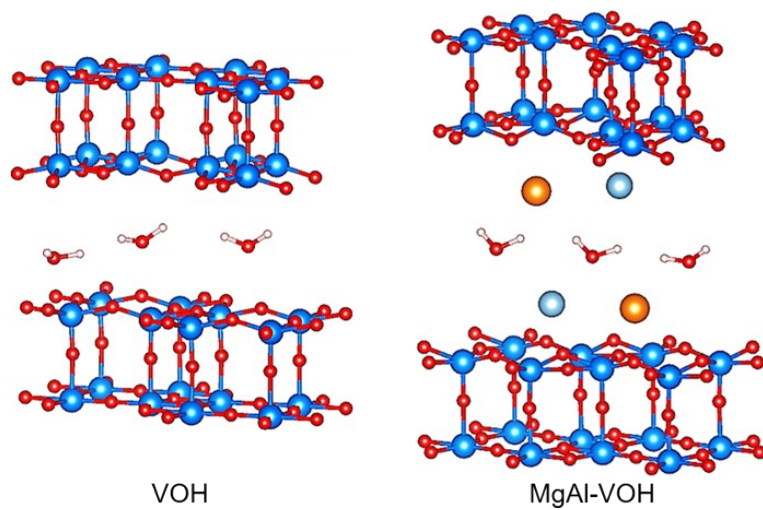
MgAl-VOH

Fig. S20 The optimized atomic models of MgAl-VOH and pure VOH, respectively.
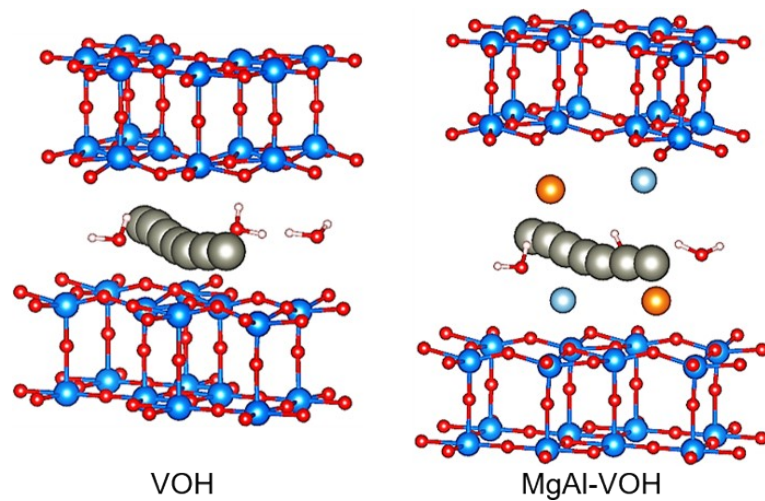
VOH MgAl-VOH

Fig. S21 The migration pathways of $Zn^{2+}$ ions in MgAl-VOH and pure VOH, respectively.

Table S1 ICP-OES results of MgAl-VOH, Mg-VOH, Al-VOH, and pure VOH.

| Sample | Element | Content |
|---|---|---|
| MgAl-VOH | Mg | 1.0% |
| | Al | 0.8% |
| | V | 42.2% |
| Mg-VOH | Mg | 1.2% |
| | V | 45.8% |
| Al-VOH | Al | 0.8% |
| | V | 45.4% |
| VOH | V | 49.3% |

Table S2 FTIR results of MgAl-VOH, Mg-VOH, Al-VOH, and pure VOH.

| Sample | Peak position (cm$^{-1}$) | FWHM (cm$^{-1}$) |
|---|---|---|
| MgAl-VOH | 1008 | 41 |
| Mg-VOH | 1007 | 56 |
| Al-VOH | 1004 | 60 |
| VOH | 1002 | 72 |

Table S3 EXAFS fitting parameters at V $K$-edge for various samples ($S0\ 2$=0.75).

| Sample | Shell | $N^{a}$ | $R$(Å)[b] | $\sigma^2$(Å$^2$)[c] | $\Delta E_0$ (eV)[d] | R factor |
|---|---|---|---|---|---|---|
| V foil | V-V | 8* | 2.61±0.01 | 0.0078±0.0065 | 3.9±0.8 | 0.007 |
| | V-V | 6* | 3.00±0.01 | 0.0075±0.0011 | | |
| MgAl-VOH | V=O | 0.7±0.5 | 1.59±0.04 | 0.0071±0.0025 | 6.0±2.6 | 0.012 |
| | V=O | 3.0±0.9 | 1.90±0.01 | | | |
| | V-V | 2.0±0.6 | 3.03±0.02 | | | |
| VOH | V=O | 0.8±0.3 | 1.65±0.02 | 0.003* | 6.0±2.4 | 0.027 |
| | V=O | 2.2±0.3 | 1.92±0.01 | | | |
| | V-V | 1.3±0.2 | 3.03±0.02 | | | |

[a]$N$: coordination number; [b]$R$: bond length; [c]$\sigma^2$: Debye-Waller factors; [d]$\Delta E_0$: inner potential correction; $R$ factor: goodness of fit. $S0\ 2$ was set to be 0.75, according to the experimental EXAFS fit of V foil by fixing CN as the known crystallographic value.

Table S4 ICP-OES results of MgAl-VOH with different $Mg^{2+}$ and $Al^{3+}$ ions concentrations.

| | MgAl-VOH-1 | MgAl-VOH | MgAl-VOH-2 | MgAl-VOH-3 | MgAl-VOH-4 |
|---|---|---|---|---|---|
| Mg | 0.6 wt% | 1.0 wt% | 1.7 wt% | 2.3 wt% | 2.4 wt% |
| Al | 0.5 wt% | 0.8 wt% | 1.6 wt% | 1.9 wt% | 2.3 wt% |

Table S5 Capacity comparison of MgAl-VOH with the other vanadium oxides at different current densities.

| Sample | Current density $(A\ g^{-1})$ | Capacity $(mAh\ g^{-1})$ | Cycling number | Reference |
|---|---|---|---|---|
| PEO-LVO | 0.1 | 438 | 3000 | 1 |
| MVOH | 0.1 | 405 | 900 | 2 |
| HVO | 0.1 | 323 | 1000 | 3 |
| NVO/PoPDA@GO | 0.5 | 433 | 1000 | 4 |
| NVOH | 0.05 | 366 | 1000 | 5 |
| MNVO | 0.1 | 410 | 5000 | 6 |
| PEDOT-NVO | 0.05 | 356 | 5000 | 7 |
| $O_v$-ZVO | 0.1 | 402 | 2000 | 8 |
| $O_d$-VO | 0.2 | 405 | 2000 | 9 |
| NaCaVO | 0.1 | 347 | 2000 | 10 |
| AlVO-DMF | 0.1 | 401 | 2000 | 11 |
| (1Zn, 1Ch)-VOH | 0.5 | 424 | 2000 | 12 |
| $CO_2$-$V_6O_{13}$ | 0.1 | 471 | 4000 | 13 |
| NiVO-BTA | 0.2 | 464 | 1600 | 14 |
| **MgAl-VOH** | **0.1** | **524** | **3000** | **This work** |

1.  M. H. Wu, C. Shi, J. W. Yang, Y. Zong, Y. Chen, Z. G. Ren, Y. X. Zhao, Z. Li, W. Zhang, L. Y. Wang, X. L. Huang, W. Wen, X. L. Li, X. Ning, X. C. Ren and D. M. Zhu, *Adv. Mater.*, 2024, **36**, 2310434.

2.  L. Yang, Y.-J. Zhu, F. L. Zeng, H.-P. Yu, L.-Y. Dong, J. C. Tao, G. He and H. Li, *Energy Storage Mater.*, 2024, **65**, 103162.

3.  N. N. Liu, X. Wu, L. S. Fan, S. Gong, Z. K. Guo, A. S. Chen, C. Y. Zhao, Y. C. Mao, N. Q. Zhang and K. N. Sun, *Adv. Mater.*, 2020, **32**, 1908420.

4.  M. Li, M. Z. Liu, Y. Y. Lu, G. D. Zhang, Y. Zhang, Z. Y. Li, Q. J. Xu, H. M. Liu and Y. G. Wang, *Adv. Funct. Mater.*, 2024, **34**, 2312789.

5.  Y. Liu, C. J. Lu, Y. T. Yang, W. S. Chen, F. Ye, H. L. Dong, Y. P. Wu, R. Z. Ma and L. F. Hu, *Adv. Mater.*, 2024, **36**, 2312982.

6.  X. R. Wang, Y. L. Wang, A. Naveed, G. T. Li, H. W. Zhang, Y. Zhou, A. C. Dou, M. R. Su, Y. J. Liu, R. Q. Guo and C. C. Li, *Adv. Funct. Mater.*, 2023, **33**, 2306205.

7.  D. Bin, W. C. Huo, Y. B. Yuan, J. H. Huang, Y. Liu, Y. X. Zhang, F. Dong, Y. G. Wang and Y. Y. Xia, *Chem*, 2020, **6**, 968–984.

8.  J.-J. Ye, P.-H. Li, H.-R. Zhang, Z.-Y. Song, T. J. Fan, W. Q. Zhang, J. Tian, T. Huang, Y. T. Qian, Z. G. Hou, N. Shpigel, L.-F. Chen and S. X. Dou, *Adv. Funct. Mater.*, 2023, **33**, 2305659.

9.  M. Liao, J. W. Wang, L. Ye, H. Sun, Y. Z. Wen, C. Wang, X. M. Sun, B. J. Wang and H. S. Peng, *Angew. Chem. Int. Ed.*, 2020, **132**, 2293–2298.

10. K. Y. Zhu, T. Wu and K. Huang, *Adv. Energy Mater.*, 2019, **9**, 1901968.

11. F. Wan, Z. M. Hao, S. Wang, Y. X. Ni, J. C. Zhu, Z. W. Tie, S. S. Bi, Z. Q. Niu and J. Chen, *Adv. Mater.*, 2021, **33**, 2102701.

12. Q. Zong, Y. L. Zhuang, C. F. Liu, Q. L. Kang, Y. Z. Wu, J. J. Zhang, J. Y. Wang, D. W. Tao, Q. L. Zhang and G. Z. Cao, *Adv. Energy Mater.*, 2023, **13**, 2301480.

13. W. Shi, B. S. Yin, Y. Yang, M. B. Sullivan, J. Wang, Y.-W. Zhang, Z. G. Yu, W. S. V. Lee and J. M. Xue, *ACS Nano*, 2021, **15**, 1273–1281.

14. J. D. Guo, J. X. Liu, W. B. Ma, Z. Y. Sang, L. C. Yin, X. Q. Zhang, H. Chen, J. Liang and D. A. Yang, *Adv. Funct. Mater.*, 2023, **33**, 2302659.